

Estimation of detection limits of a clinical fluorescence optical mammography system for the near-infrared fluorophore IRDye800CW: phantom experiments

Arthur Adams
Jurgen E. M. Mourik
Marjolein van der Voort
Paul C. Pearlman
Tim Nielsen
Willem P. Th. M. Mali
Sjoerd G. Elias

Estimation of detection limits of a clinical fluorescence optical mammography system for the near-infrared fluorophore IRDye800CW: phantom experiments

Arthur Adams,^a Jurgen E. M. Mourik,^{b,c} Marjolein van der Voort,^d Paul C. Pearlman,^b Tim Nielsen,^e Willem P. Th. M. Mali,^a and Sjoerd G. Elias^{a,f}

^aUniversity Medical Center Utrecht, Department of Radiology, Utrecht, The Netherlands

^bUniversity Medical Center Utrecht, Image Science Institute, Utrecht, The Netherlands

^cLeiden University Medical Center, Department of Radiology, Leiden, The Netherlands

^dPhilips Research, Eindhoven, The Netherlands

^ePhilips Research, Hamburg, Germany

^fUniversity Medical Center Utrecht, Julius Center of Health Sciences and Primary Care, Utrecht, The Netherlands

Abstract. To evaluate if clinical fluorescence imaging of IRDye800CW is feasible on our fluorescence optical mammography system by estimating detection limits assessed by breast-cancer-simulating phantom experiments. Phantoms (2.1 cm³, 0.9 cm³) with IRDye800CW concentrations of 0.5 to 120 nM were suspended in a 550 cm³ measurement cup containing 507 surface-mounted source and detector fibers. The cup was filled with optical matching fluid containing IRDye800CW concentrations of 0, 5, 10, or 20 nM. Tomographic fluorescence images were acquired by exciting IRDye800CW at 730 nm; wavelengths above 750 nm were filtered. Signal intensities were calculated over a volume of interest corresponding to the size and location of the phantom in the reconstructed images. Correlations (R^2) were calculated, and detection limits with associated upper 95% prediction interval were estimated. Between-day reproducibility was assessed with intraclass correlation coefficients (ICC). Fluorescent intensities were strongly correlated with phantom IRDye800CW concentrations (R^2 : 0.983 to 0.999). IRDye800CW detection limits ranged from 0.14 to 2.46 nM (upper 95% prediction limit 4.63 to 18.63 nM). ICC ranged from 0.88 to 1.00. The estimated detection limits for IRDye800CW were in the low-nanomolar range. These results support the start of clinical trials to evaluate the fluorescence optical mammography system using IRDye800CW labeled breast cancer targeting ligands. © 2012 Society of Photo-Optical Instrumentation Engineers (SPIE). [DOI: 10.1117/1.JBO.17.7.076022]

Keywords: molecular imaging; near-infrared fluorescence optical mammography; IRDye800CW; phantom experiments; detection limits.

Paper 12155 received Mar. 5, 2012; revised manuscript received Jun. 14, 2012; accepted for publication Jun. 21, 2012; published online Jul. 17, 2012.

1 Introduction

Breast cancer is the most common type of cancer and the second leading cause of death of women in the western world.¹ The currently used imaging modalities, including (digital) x mammography, ultrasound, and dynamic contrast enhanced magnetic resonance imaging, play a vital role in the detection and evaluation of breast lesions.²⁻⁵ However, each of these modalities has limitations, such as moderate sensitivity or specificity for breast cancer detection, high costs, the use of ionizing radiation, or painful compression of the breast. Molecular imaging of the breast is a promising emerging technology that visualizes breast-cancer-specific molecular alterations already present during early carcinogenesis. With molecular imaging, breast disease may be detected even before the anatomical changes necessary for visualization with current imaging modalities occur, making it valuable for early detection and characterization of breast cancer. Molecular imaging with breast cancer targeting ligands conjugated to fluorescent molecules has advantages when compared to other molecular imaging modalities. Sensitivity for fluorophores is at least a hundred to a

thousand times higher as compared to contrast agents used in MRI and computed tomography.⁶ In contrast to nuclear medicine techniques, patients are not exposed to harmful ionizing radiation, and there is no need for an expensive and complex infrastructure. Furthermore, acquisitions can be performed fast, making repeated, non-invasive measurements possible. Especially of interest are fluorophores with absorption and emission spectrums in the near infrared range that yield sufficient tissue penetration for breast imaging even in dense breast tissue, where x-ray mammography has limited value.^{2,7}

Until now, only two fluorophores, indocyanin green (ICG) and omocyanine, have been used in clinical fluorescence imaging studies of breast diseases.⁸⁻¹⁶ However, the fluorophores used in these studies can not be conjugated to a (breast cancer) targeting ligand, and tend to bind non-specifically to serum proteins. Accumulation of the fluorophore in the tumor tissue thus solely depends on increased blood content due to tumor angiogenesis and the enhanced permeability and retention effect. The results of these studies were promising, but specificity was low due to nonspecific accumulation of the fluorophore in healthy tissue.

The near infrared fluorophore IRDye800CW (LI-COR, NE) has a reactive group for conjugation to a range of targeting

Address all correspondence to: A. Adams, University Medical Center Utrecht, Department of Radiology, P.O. Box 85500 HP E01.132, 3508 GA Utrecht, The Netherlands. Tel: +31 88 7550580/+31 88 7556689; Fax: +31 302581098; E-mail: a.adams@umcutrecht.nl.

ligands and has a 1.3 to 7.4 times higher quantum yield compared to ICG.¹⁷⁻²⁰ Animal data indicate that IRDye800CW is nontoxic, and it has been successfully used in conjunction with breast cancer relevant monoclonal antibodies in a preclinical study.^{21,22} Recently, it has been approved for administration to humans in molecular imaging trials. Administration of IRDye800CW-labeled ligands could greatly improve the performance of fluorescence molecular imaging systems.

In a clinical study performed at our institution, a fluorescence optical mammography system was able to visualize accumulation of the fluorophore omocyanin in patients with breast cancer.^{16,23,24} In upcoming molecular fluorescence imaging trials, it is expected that accumulation of IRDye800CW, having a higher quantum yield, can be visualized with our system, as well. However, the administered doses of IRDye800CW targeted ligands will be lower, resulting in an expected lower absolute amount of the fluorophore in the tumor tissue, but with higher concentration differences between tumor and background. Also, the excitation wavelength for this system [730 nanometer (nm)] is specifically chosen to minimize absorption by breast tissue to increase imaging depth, and is therefore not aligned towards the optimal excitation wavelength of IRDye800CW (774 nm). Given these uncertainties, it was necessary to empirically assess the detection limits of this system for IRDye800CW. We performed extensive breast cancer simulating phantom experiments to conclude if imaging of this fluorescent dye is feasible in patients in nanomolar concentrations.

2 Fluorescence Optical Mammography System

The properties of our fluorescence optical mammography system (Philips, Eindhoven, The Netherlands) used for the experiments have previously been described extensively.²⁵ The scanning module consists of a scanner bed with a cup-shaped measurement chamber, containing 507 surface-mounted optical fibers [Fig. 1(a)]. In transmission mode, 253 source fibers direct the light of four continuous wave solid-state laser diodes at wavelengths of 690, 730, 780, and 850 nm into the measurement cup. The source fibers are interleaved with 254 fibers to detect the light emanating from the breast simultaneously from each source fiber. The light is detected by photodiodes (S2386-18K, Hamamatsu, Bridgewater, NJ) that are connected to a custom-made readout circuit. In fluorescence mode, signal intensities can be acquired by exciting the fluorophore with the laser at 730 nm and filtering out light of 750 nm and higher with a long-pass filter. This excitation wavelength differs from the optimal excitation wavelength for IRDye800CW (774 nm), but was estimated to be in the wavelength range where absorption of breast tissue is minimal, in order to maximize penetration of the light to several centimeters of tissue, which is necessary given the cup geometry of the system.²⁶ Measurement cups are available in several sizes with volumes ranging from 300 to 1100 cm³ to allow breasts of different sizes to fit. For a typical scan, a patient lies prone on the scanner bed with one breast in the measurement cup. The remainder of the cup is then filled with an optical matching fluid to enable stable coupling between

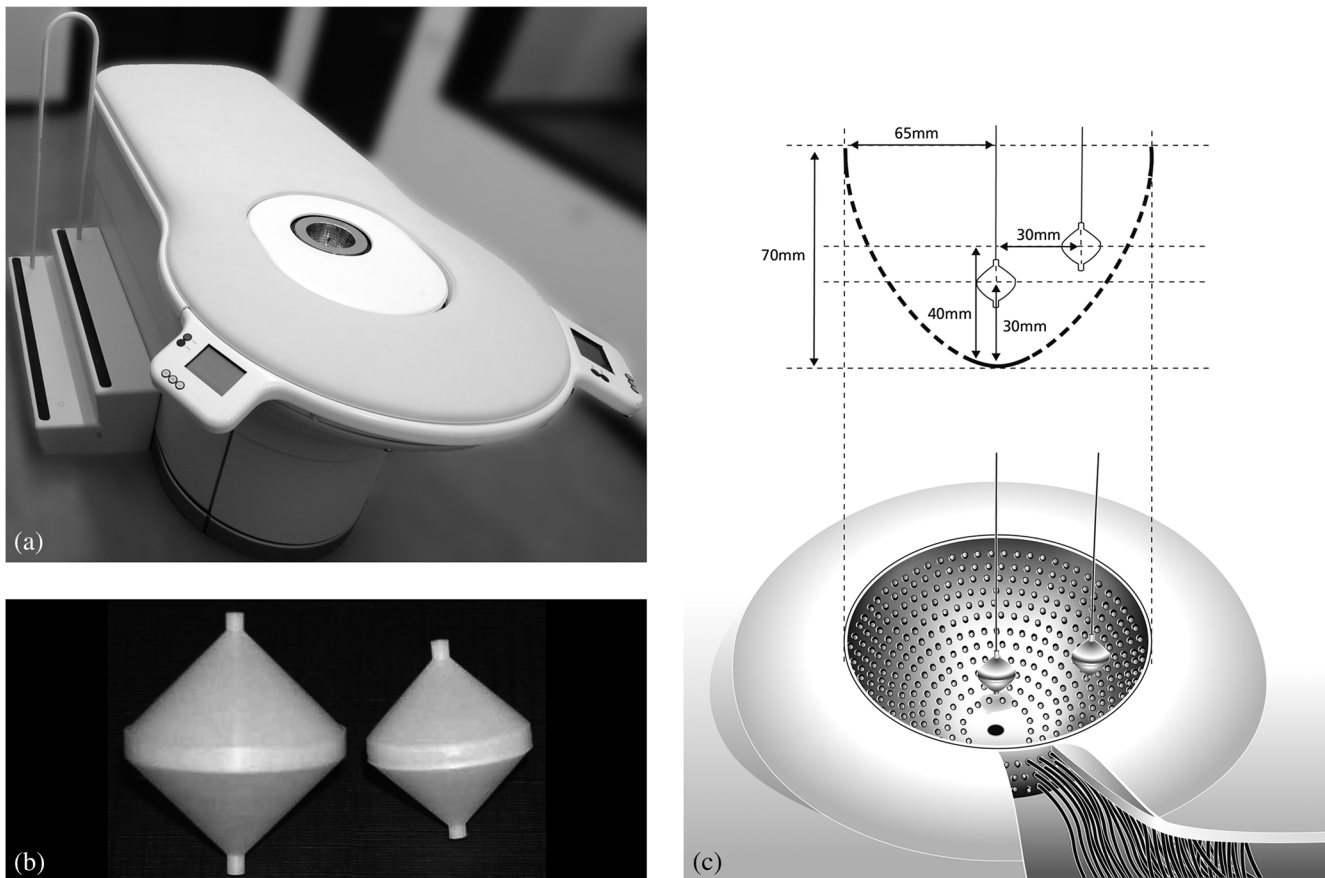


Fig. 1 (a) The fluorescence optical mammography system (Philips, Eindhoven, The Netherlands). (b) Phantom shapes used for the experiments, made of polyoxymethylene. Left: large phantom (diameter 20 mm, volume: 2.1 cm³); right: small phantom (diameter 15 mm, volume 0.9 cm³). (c) Locations of the phantom shapes in the measurement cup of the fluorescence optical mammography system.

fibers and the breast and to eliminate shortcuts of the light around the breast.

3 Phantom Experiments

IRDye800CW (LI-COR, NE) (peak absorption 774 nm, peak emission 789 nm) was mixed with optical matching fluid in various concentrations. The optical matching fluid contains low-density particles (hollow glass spheres) to mimic the average scattering properties, and light-absorbing dyes to mimic the average absorption properties of breast tissue.²⁶ The optical properties of the matching fluid were: attenuation coefficients (μ_a): 3.4 m^{-1} (690 nm), 3.1 m^{-1} (730 nm), 3.8 m^{-1} (780 nm), 5.1 m^{-1} (850 nm), and reduced scattering coefficients (μ_s'): $1.2 \times 10^{-3} \text{ m}^{-1}$ (690 nm), $1.2 \times 10^3 \text{ m}^{-1}$ (730 nm), $1.1 \times 10^3 \text{ m}^{-1}$ (780 nm), $1.0 \times 10^3 \text{ m}^{-1}$ (850 nm). Hollow, double-cone shaped phantoms made of polyoxymethelene were filled with these mixtures of optical matching fluid and IRDye800CW. Two phantom sizes were used: a large phantom of 20-mm diameter (2.1 cm^3), and a small phantom of 15-mm diameter (0.9 cm^3), corresponding to a small T2 and T1c breast tumor, respectively [Fig. 1(b)]. The phantoms were suspended on a thin wire in a measurement cup of 550 cm^3 on two locations: close to the wall of the measurement cup (superficial position) or in the center of the measurement cup (deep position) [Fig. 1(c)]. The remainder of the measurement cup was filled with a mixture of the optical fluid and IRDye800CW in concentrations of 0, 5, 10 or 20 nanomolar (nM) (background concentrations). This setup simulates a situation in which a breast with homogeneous optical properties perfectly fits in the measurement cup and includes a single tumor in which the fluorophore has accumulated, and where various concentrations of the fluorophore are present in surrounding tissue mimicking non-specific uptake.

Tomographic fluorescence acquisitions were obtained for each combination of phantom size, phantom location, and fluorophore concentration in the phantom and in the surrounding optical matching fluid. Concentrations of IRDye800CW in the phantom ranged from 0.5 to 120.0 nM in 0 nM, 7.0 to 30.0 nM in 5 nM, 12.0 to 60.0 nM in 10 nM, and 22.0 to 120.0 nM in 20 nM background concentration, respectively. Five acquisitions with equal concentrations of fluorophore in the phantom shape and the surrounding optical matching fluid ('blank' measurements) were performed to assess background noise levels in the reconstructed images for each situation, necessary to calculate limits of detection. All measurements were repeated two months later.

4 Image Reconstruction and Analysis

Three-dimensional (3-D) fluorescence images were reconstructed using algorithms based on the Born approximation with the same parameters that are used for reconstruction of acquisitions of the human breast.²⁷ Average signal intensities were obtained from a volume of interest corresponding to the size and location of the phantom. Then, signal intensities of the blank measurements were subtracted to obtain signal intensity differences.

Least squares linear regression lines were fit through the obtained signal intensities for the investigated phantom concentration ranges and the explained variance (R^2) based on the Pearson's correlation coefficients was calculated. Reproducibility was determined with intraclass correlation coefficients (ICC) and associated 95% confidence intervals. The limit of detection (LOD), defined as the minimal concentration difference of

IRDye800CW that can be detected in a phantom above background noise, was estimated using the formula $\text{LOD} = 3.3 * s_B / \beta$, where s_B is the standard deviation of the (five) blank measurements and β is the least squares linear regression coefficient obtained from the calibration curves. The chosen multiplication factor of 3.3 limits the type-I and type-II error to 5%.²⁸ To provide a conservative estimate of the LOD taking into account the statistical uncertainty in our measurements, the upper limit of the 95% prediction interval for concentrations compatible with a fluorescence signal of $3.3 * s_B$ were calculated.

The software package R version 2.14.0 (R Foundation for Statistical Computing, Vienna, Austria) with the package 'chemCal' version 0.1-27 (J. Ranke, University Bremen, Bremen, Germany) was used for the statistical computations.

5 Results

A total of 344 measurements were performed. A strong linear relation was found between IRDye800CW concentrations and signal intensities for all different conditions regarding phantom size, phantom location, and background concentration, with R^2 ranging from 0.983 to 0.999. Phantoms located superficially yielded higher signal intensities and signal intensities were consistently higher for the large phantom compared to the small phantom, regardless of location [Fig. 2(a) to 2(d)].

Despite large differences in the various investigated situations, all detection limits were estimated in the same, low nanomolar range. Detection limits tended to be slightly higher for higher background IRDye800CW concentrations (due to higher noise levels) and for smaller and deeply located phantoms (due to a lower obtained signal intensity). Detection limits ranged from 0.14 nM (upper 95% prediction limit 4.63 nM) for a large, deeply located phantom in a background concentration of 0 to 2.46 nM (upper 95% prediction limit 18.63 nM) for a small, deeply located phantom in a background concentration of 20 nM.

Reproducibility of the measurements was excellent in all situations, with ICC ranging from 0.88 to 1.00. The results are summarized in Table 1. A sample of images of a large, superficially located phantom containing four different concentrations of IRDye800CW (10, 20, 30, and 60 nM) in a background concentration of 10 nM is shown in Fig. 3.

6 Discussion

In this study, the detection limits of the fluorescence optical mammography system for IRDye800CW were estimated in the low-nanomolar range for all investigated situations. The upper 95% prediction limit of the LOD yielded conservative estimates between 3.18 and 18.63 nM, taking into account the statistical uncertainty in our data. With an experimental setup that approaches a clinical situation (e.g., an optical medium that has comparable optical properties as to breast tissue, phantom volumes comparable to breast tumor volumes commonly found in clinical practice, and phantoms suspended at feasible locations for breast tumors), and with a high number of measurements, a strong linear correlation between true IRDye800CW concentrations and measured fluorescence signal intensity was found with a high reproducibility, enabling us to adequately estimate detection limits. This indicates the potential of the fluorescence optical mammography system to visualize IRDye800CW labeled ligands in humans.

There are several approaches possible to further improve sensitivity of the fluorescence optical mammography system for IRDye800CW. For example, it has already been shown that

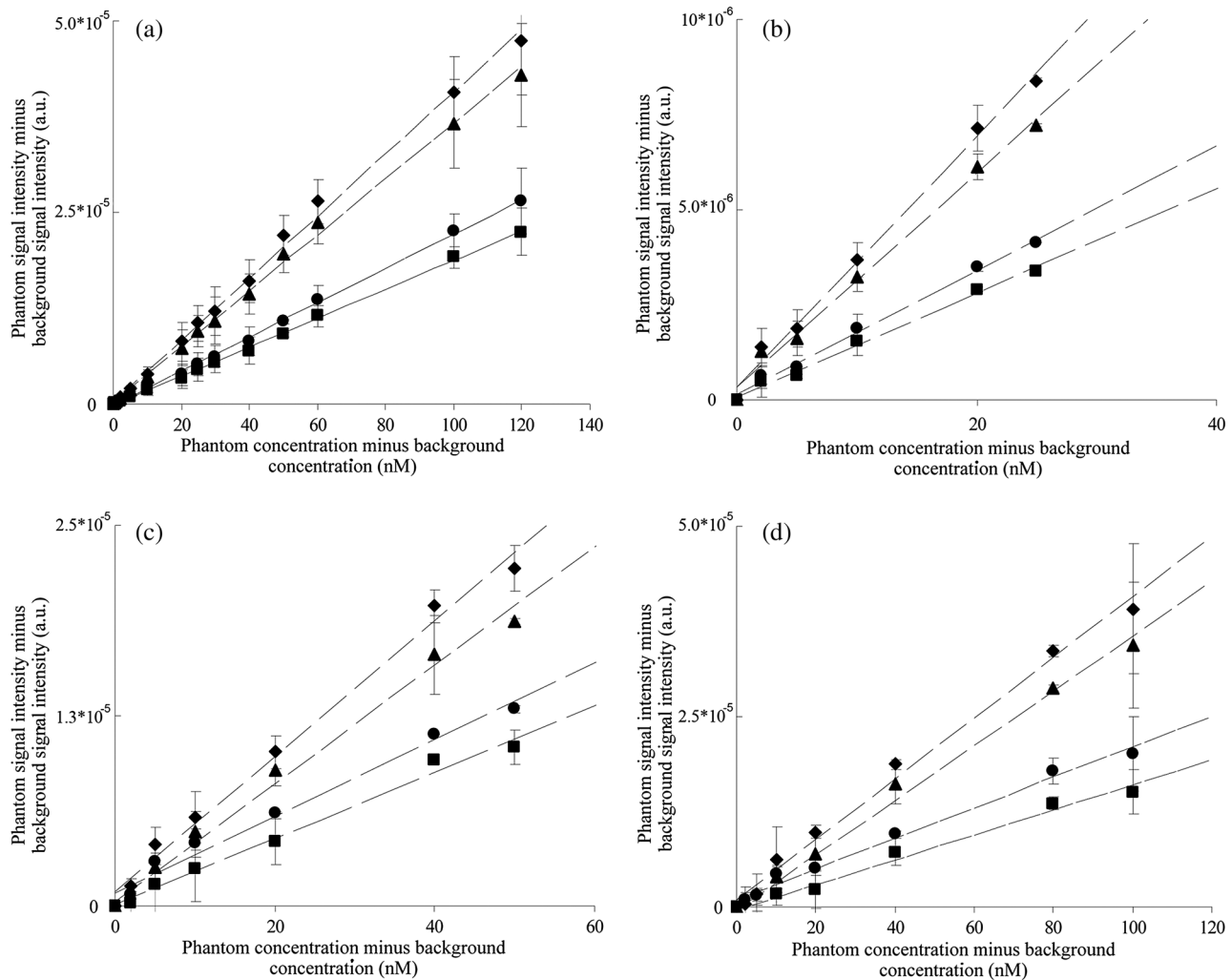


Fig. 2 Results of fluorescence measurements with a background IRDye800CW concentration of (a) 0 nM, (b) 5 nM, (c) 10 nM, and (d) 20 nM. Error bars represent the standard deviation of duplicate measurements. \blacklozenge : large phantom, superficial position; \blacktriangle : large phantom, deep position; \bullet : small phantom, superficial position; \blacksquare : small phantom, deep position; a.u.: arbitrary units.

by combining fluorescence and absorption information, phantoms with a low concentration of a fluorophore suspended at an unknown location can be detected that were not visible in the fluorescence images alone.²⁹ Furthermore, no *a priori* information was used for reconstruction of the images. By coregistration or hybrid acquisition with an anatomical imaging modality, size, location, and other structural differences could be used as priors for the reconstruction of the optical images, improving image quality, reducing the presence of artifacts and facilitating image interpretation. Adaptation of current laser (730 nm) and filtering (750 nm) wavelengths towards the optimal absorption wavelength (e.g., 774 nm) and emission wavelength (e.g., 789 nm) of IRDye800CW could improve performance of our system as well. In particular, tumors located superficially in the breast would benefit from this adaptation. On the other hand, for tumors that would be located deeply in the breast (e.g., at a depth of several centimeters), this could have a negative impact, as a significant amount of photons at these wavelengths will be absorbed by breast tissue itself, resulting in lower obtained signal intensities.^{26,30} As breast cancer rarely presents at superficial locations, and given the cup geometry of our system, we considered light penetration

depth to be more important than optimal IRDye800CW excitation. The chosen laser wavelength of 730 nm was therefore an estimation of the best excitation wavelength. However, other wavelengths could perform even better depending on image acquisition geometry and application. Last, the use of photomultipliers instead of photodiodes to detect light intensities could be considered, as the signal intensities that are obtained will be more amplified, thus possibly improving detection limits. However, this advantage is limited by higher noise levels, and a lower conversion efficacy of photomultipliers in the near infrared range.

Several factors that will likely influence detection limits in human investigations could not be taken into account in our phantom experiments study. For example, a homogenous optical matching fluid was used to mimic breast tissue, whereas real breast tissue will have inhomogeneities due to breast specific structures such as blood vessels, the nipple, skin colour alterations, and structural changes due to breast carcinogenesis. A high breast density (resulting in more absorption by breast tissue), large breast size (increasing the path length of the light), patient movement, heartbeat and breathing during the acquisition will further affect the acquisition of a fluorescent signal.

Table 1 Results.

Background IRDye800CW concentration (nM)	Phantom size	Phantom location	Calibration coefficient (β)	S_b	LOD (nM)	Upper 95% prediction limit (nM)	ICC (95% confidence interval) ^a	R^2
0	Large	Superficial	4.04×10^{-7}	1.90×10^{-8}	0.16	5.35	0.96 (0.89–0.99)	0.997
		Deep	3.64×10^{-7}	1.51×10^{-8}	0.14	4.63	0.95 (0.86–0.99)	0.998
	Small	Superficial	2.24×10^{-7}	2.50×10^{-8}	0.37	3.81	0.96 (0.89–0.99)	0.999
		Deep	1.89×10^{-7}	2.25×10^{-8}	0.39	3.74	0.97 (0.90–0.99)	0.999
5	Large	Superficial	3.19×10^{-7}	1.71×10^{-8}	0.18	3.18	0.98 (0.85–1.00)	0.996
		Deep	2.71×10^{-7}	3.84×10^{-8}	0.47	3.80	0.98 (0.84–1.00)	0.995
	Small	Superficial	1.59×10^{-7}	2.68×10^{-8}	0.56	3.73	0.96 (0.67–1.00)	0.995
		Deep	1.34×10^{-7}	4.44×10^{-8}	1.09	5.23	0.93 (0.49–1.00)	0.993
10	Large	Superficial	4.34×10^{-7}	1.55×10^{-7}	1.18	7.58	0.99 (0.97–1.00)	0.992
		Deep	3.86×10^{-7}	8.94×10^{-8}	0.77	10.21	0.97 (0.80–1.00)	0.983
	Small	Superficial	2.43×10^{-7}	3.54×10^{-8}	0.48	9.34	0.99 (0.92–1.00)	0.985
		Deep	2.17×10^{-7}	1.14×10^{-7}	1.73	9.73	0.88 (0.43–0.98)	0.988
20	Large	Superficial	3.95×10^{-7}	9.25×10^{-8}	0.77	12.41	0.94 (0.72–0.99)	0.991
		Deep	3.61×10^{-7}	6.61×10^{-8}	0.60	12.25	0.94 (0.73–0.99)	0.991
	Small	Superficial	1.97×10^{-7}	8.09×10^{-8}	1.35	14.12	0.93 (0.69–0.99)	0.990
		Deep	1.67×10^{-7}	1.25×10^{-7}	2.46	18.63	0.90 (0.59–0.98)	0.983

^aOne-way random effects model where day effects are random, single measures; ICC: intraclass correlation coefficient; LOD: limit of detection; S_b : standard deviation of 5 blank measurements.

Also, a volume of interest with a fixed size and location matching the experiment to derive the signal intensity from was used in our study, where in clinical breast imaging the exact location and size of the volume of interest is not known. These factors will likely negatively affect the LOD in clinical trials compared to our standardized and comprehensive phantom experiments. Nevertheless, even if the true LOD is about 10 times higher in human investigations, the performance of the system is still likely to be relevant in clinical situations.^{6,31}

Other groups have explored the capabilities of their optical imaging systems and contrast agents with phantom experiments

as well. The SoftScan system (Advanced Research Technologies Inc., Canada) was used to visualize highly absorbing contrast agents.³² Single-walled carbon nanotubes were visible in a concentration of 0.8 nM and a Black Hole Quencher was visible in a concentration of 8.0 μ M in phantoms with a volume of 0.2 cm³. In phantom experiments with a frequency-domain handheld probe-based optical imager developed by the group of Godavarty, concentrations of ICG of 1.0 μ M were detectable in small phantoms of 0.10 to 0.45 cm³ at a depth of 2.5 cm, but large relative differences in phantom-to-background concentrations (up to 25:1) and high baseline concentrations of the

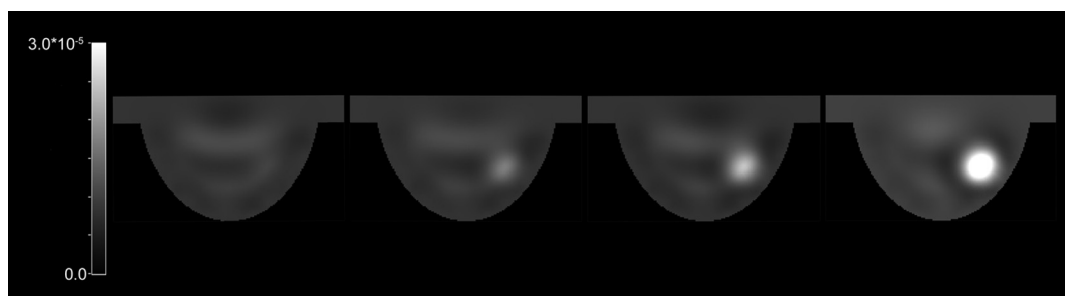


Fig. 3 Example of reconstructed fluorescence images with a large phantom suspended at a superficial position. The concentration of IRDye800CW in the background was 10 nM, with concentrations of IRDye800CW in the 2.1 cm³ phantom of 10 nM, 20 nM, 30 nM, and 60 nM, respectively (left to right).

fluorophore (1.0 μM) were required for detection.^{33,34} With opto-acoustic imaging, optical contrast can be resolved up to centimetres of tissue depth with resolutions achieved by ultrasound imaging.³⁵ A system developed by the group of Ntziachristos was able to obtain opto-acoustic signals of a phantom with a size of 0.5-cm diameter and a concentration of 5.0 μM of the fluorophore Cy5.5 up to a depth of 3.0 cm.³⁶ Above indicates the variability in detection limits between the various fluorescence imaging systems, depending on application area, the used fluorophore, excitation wavelengths, laser powers, desired light penetration depth, number of used sources and detectors and various other factors.

In conclusion, we have shown that our clinical fluorescence optical mammography system is able to detect low nanomolar concentration differences of IRDye800CW in a breast-cancer-simulating phantom study. IRDye800CW-labeled breast cancer targeting ligands are at the brink of clinical evaluation, for example, by using readily available and clinically used antibodies. As previous clinical trials have indicated that non-targeted fluorescence optical breast cancer imaging is feasible, it is expected that our clinical fluorescence optical mammography system has high potential to visualize molecular processes associated with breast cancer after administration of such cancer-specific IRDye800CW-labeled ligands.

Acknowledgments

This research was supported by the Center for Translational Molecular Medicine - Mammary Carcinoma Molecular Imaging for Diagnosis and Therapeutics (CTMM—MAMMOTH) project, and by the Dutch Cancer Society KWF by a research fellowship to S.G.E. The authors thank S. Oliveira for her assistance with the preparations of the IRDye800CW dilutions.

References

- J. Ferlay et al., "Estimates of worldwide burden of cancer in 2008: GLOBOCAN 2008," *Int. J. Cancer* **127**(12), 2893–2917 (2010).
- P. C. Gotzsche and M. Nielsen, "Screening for breast cancer with mammography," *Cochrane Database Syst. Rev.* (1), CD001877 (2011).
- R. J. Hooley, L. Andrejeva, and L. M. Scoult, "Breast cancer screening and problem solving using mammography, ultrasound, and magnetic resonance imaging," *Ultrasound Q.* **27**(1), 23–47 (2011).
- N. H. Peters et al., "Meta-analysis of MR imaging in the diagnosis of breast lesions," *Radiology*. **246**(1), 116–124 (2008).
- M. Morrow, J. Waters, and E. Morris, "MRI for breast cancer screening, diagnosis, and treatment," *Lancet*. **378**(9805), 1804–1811 (2011).
- J. V. Frangioni, "New technologies for human cancer imaging," *J. Clin. Oncol.* **26**(24), 4012–4021 (2008).
- V. Ntziachristos, C. Bremer, and R. Weissleder, "Fluorescence imaging with near-infrared light: new technological advances that enable in vivo molecular imaging," *Eur. Radiol.* **13**(1), 195–208 (2003).
- X. Intes et al., "In vivo continuous-wave optical breast imaging enhanced with Indocyanine Green," *Med. Phys.* **30**(6), 1039–1047 (2003).
- D. Grosenick et al., "A multichannel time-domain scanning fluorescence mammograph: performance assessment and first in vivo results," *Rev. Sci. Instrum.* **82**(2), 024302 (2011).
- A. Hagen et al., "Late-fluorescence mammography assesses tumor capillary permeability and differentiates malignant from benign lesions," *Opt. Express* **17**(19), 17016–17033 (2009).
- A. Poellinger et al., "Near-infrared imaging of the breast using omocyanine as a fluorescent dye: results of a placebo-controlled, clinical, multicenter trial," *Invest. Radiol.* **46**(11), 697–704 (2011).
- A. Poellinger et al., "Breast cancer: early- and late-fluorescence near-infrared imaging with indocyanine green—a preliminary study," *Radiology* **258**(2), 409–416 (2011).
- P. Schneider et al., "Fast 3D Near-infrared breast imaging using indocyanine green for detection and characterization of breast lesions," *Rofo*. **183**(10), 956–963 (2011).
- V. Ntziachristos et al., "Concurrent MRI and diffuse optical tomography of breast after indocyanine green enhancement," *Proc. Natl. Acad. Sci. U. S. A.* **97**(6), 2767–2772 (2000).
- A. Corlu et al., "Three-dimensional in vivo fluorescence diffuse optical tomography of breast cancer in humans," *Opt. Express* **15**(11), 6696–6716 (2007).
- S. Van de Ven et al., "A novel fluorescent imaging agent for diffuse optical tomography of the breast: first clinical experience in patients," *Mol. Imag. Biol.* **12**(3), 343–348 (2010).
- S. Ohnishi et al., "Organic alternatives to quantum dots for intraoperative near-infrared fluorescent sentinel lymph node mapping," *Mol. Imag.* **4**(3), 172–181 (2005).
- E. Tanaka et al., "Image-guided oncologic surgery using invisible light: completed pre-clinical development for sentinel lymph node mapping," *Ann. Surg. Oncol.* **13**(12), 1671–1681 (2006).
- C. Kim, C. Favazza, and L. V. Wang, "In vivo photoacoustic tomography of chemicals: high-resolution functional and molecular optical imaging at new depths," *Chem. Rev.* **110**(5), 2756–2782 (2010).
- Y. Ashitate et al., "Real-time simultaneous near-infrared fluorescence imaging of bile duct and arterial anatomy," *J. Surg. Res.* **176**(1), 7–13 (2011).
- M. V. Marshall et al., "Single-dose intravenous toxicity study of IRDye 800CW in Sprague-Dawley rats," *Mol. Imaging Biol.* **12**(6), 583–594 (2010).
- A. G. Terwisscha van Scheltinga et al., "Intraoperative near-infrared fluorescence tumor imaging with vascular endothelial growth factor and human epidermal growth factor receptor 2 targeting antibodies," *J. Nucl. Med.* **52**(11), 1778–1785 (2011).
- S. Van de Ven et al., "Diffuse optical tomography of the breast: initial validation in benign cysts," *Mol. Imaging Biol.* **11**(2), 64–70 (2009).
- S. Van de Ven et al., "Diffuse optical tomography of the breast: preliminary findings of a new prototype and comparison with magnetic resonance imaging," *Eur. Radiol.* **19**(5), 1108–1113 (2009).
- T. Nielsen et al., "Linear image reconstruction for a diffuse optical mammography system in a noncompressed geometry using scattering fluid," *Appl. Opt.* **48**(10), D1–D13 (2009).
- L. Spinelli et al., "Bulk optical properties and tissue components in the female breast from multiwavelength time-resolved optical mammography," *J. Biomed. Opt.* **9**(6), 1137–1142 (2004).
- E. Scherleitner and B. G. Zagar, "Optical tomography imaging based on higher order Born approximation of diffuse photon density waves," *IEEE Trans. Instrum. Meas.* **54**(4), 1607–1611 (2005).
- E. Desimoni and B. Brunetti, "About estimating the limit of detection of heteroscedastic analytical systems," *Anal. Chim. Acta* **655**(1–2), 30–37 (2009).
- A. Leproux et al., "Optical mammography combined with fluorescence imaging: lesion detection using scatterplots," *Biomed. Opt. Express* **2**(4), 1007–1020 (2011).
- B. J. Tromberg et al., "Non-invasive in vivo characterization of breast tumors using photon migration spectroscopy," *Neoplasia* **2**(1–2), 26–40 (2000).
- V. Ntziachristos, "Fluorescence molecular imaging," *Annu. Rev. Biomed. Eng.* **8**, 1–33 (2006).
- S. Van de Ven et al., "Molecular imaging using light-absorbing imaging agents and a clinical optical breast imaging system—a phantom study," *Mol. Imaging Biol.* **13**(2), 232–238 (2011).
- S. J. Erickson et al., "Improved detection limits using a hand-held optical imager with coregistration capabilities," *Biomed. Opt. Express* **1**(1), 126–134 (2010).
- J. Ge, S. J. Erickson, and A. Godavarty, "Multi-projection fluorescence optical tomography using a handheld-probe-based optical imager: phantom studies," *Appl. Opt.* **49**(23), 4343–4354 (2010).
- V. Ntziachristos and D. Razansky, "Molecular imaging by means of multispectral optoacoustic tomography (MSOT)," *Chem. Rev.* **110**(5), 2783–2794 (2010).
- D. Razansky, J. Baeten, and V. Ntziachristos, "Sensitivity of molecular target detection by multispectral optoacoustic tomography (MSOT)," *Med. Phys.* **36**(3), 939–945 (2009).